AGU PUBLICATIONS

JGR

Journal of Geophysical Research: Atmospheres

RESEARCH ARTICLE
10.1002/2017JD026911

Key Points:
- Results demonstrate a link between the early and more pronounced 2015 Saharan Air Layer intrusions into the Caribbean and the suppression of the early rainfall season in Puerto Rico
- The Saharan Air Layer is identified by an anomalously low Gálvez-Davison Index, stronger trade wind inversion, and increased aerosol loadings and is associated with reduced early season rainfall in the eastern Caribbean

Correspondence to:
T. L. Mote,
tmote@uga.edu

Citation:
Mote, T. L., Ramseyer, C. A., & Miller, P. W. (2017). The Saharan Air Layer as an early rainfall season suppressant in the eastern Caribbean: The 2015 Puerto Rico drought. *Journal of Geophysical Research: Atmospheres*, *122*, 10,966–10,982. https://doi.org/10.1002/2017JD026911

Received 4 APR 2017
Accepted 8 OCT 2017
Accepted article online 12 OCT 2017
Published online 30 OCT 2017

The Saharan Air Layer as an Early Rainfall Season Suppressant in the Eastern Caribbean: The 2015 Puerto Rico Drought

Thomas L. Mote[1], Craig A. Ramseyer[2], and Paul W. Miller[1]

[1]Department of Geography, University of Georgia, Athens, GA, USA, [2]Department of Geography and Geosciences, Salisbury University, Salisbury, MD, USA

Abstract Eastern Puerto Rico and the surrounding Caribbean experienced a severe drought in 2015 that resulted in record-low reservoir and river levels. Rainfall deficits in April and May, which represent the period when the drought began, were more severe in 2015 than recent droughts of record. While El Niño has been associated with drought in the Caribbean, onset of the 2015 drought was strongly associated with lower-than-average values of a recently developed tool used by weather forecasters in San Juan, the Gálvez-Davison Index (GDI), which is used to measure the potential for thunderstorm development and rainfall. Persistently low GDI values indicate strong and frequent intrusions of hot, dry air in the low to middle troposphere, suppressing convection, both locally and in development regions for tropical waves that impact Puerto Rico. The Saharan Air Layer (SAL) is largely responsible for this anomalously hot, dry air, which produced thermodynamically stable conditions and limited thunderstorms and rainfall. Moreover, higher-than-normal aerosol concentrations, typically associated with SAL intrusion over the Caribbean, were recorded in April and May 2015. A comparison to advanced very high resolution radiometer aerosol optical thickness demonstrates that higher Caribbean aerosols in the early rainfall season, particularly June, are associated with decreased rainfall in eastern Puerto Rico. Results here demonstrate a direct link between the early and more pronounced SAL intrusions into the Caribbean and the suppression of the early rainfall season. More broadly, a reduction in the GDI and increase in the trade wind inversion was associated with reduced early season rainfall in the eastern Caribbean.

Plain Language Summary The eastern Caribbean, and specifically eastern Puerto Rico, suffered a severe drought in 2015. While discussion in the media and among professionals indicated the drought was associated with El Nino, the role of Saharan dust received relatively little attention. This research demonstrates that Saharan dust arrived early in the Caribbean in 2015 and resulted in conditions that were unfavorable for rainfall. Further analysis demonstrates that the early rainfall season (April-July) in eastern Puerto Rico is strongly related to conditions associated with Saharan dust intrusions, which were identified using a tool commonly used by operational weather forecasters in Puerto Rico.

1. Introduction

Eastern Puerto Rico, including the San Juan metropolitan area and the nearby Luquillo Mountains, suffered a drought in 2015 that caused severe water shortages and water rationing for hundreds of thousands of residents (Alvarez, 2015). At the peak of the drought in early August, only three of the island's 77 municipalities were not included in the drought, and the island experienced its first "extreme drought" recorded by the U.S. Drought Monitor (National Drought Mitigation Center, 2016). The percentage of the island classified as "moderate to severe drought" reached almost 45%, while just over 20% had moved into the more intense rating of extreme drought by early August (U.S. Department of Agriculture (USDA), 2015). Puerto Rico's agricultural sector losses topped $12 million by early August and cost the Puerto Rico Aqueduct and Sewer Authority (Autoridad de Acueductos y Alcantarillados) as much as $15 million a month (USDA, 2015).

U.S. Geological Survey (USGS) flow rates for the Rio de Bayamon registered 4% of historic flows, and the Rio Piedras and the Rio Grande de Loiza reached record lows at or below 3% of their historic average flows (USDA, 2015). The USGS classifies anything below the 5th percentile to be "severe hydrologic drought." Key reservoirs registered at or below levels associated with historic droughts such as that of 1994 (U.S. Geological Survey (USGS), 2016). USGS-computed median runoff for the island was at the 5.48 percentile in 2015, the lowest since the drought of record in 1994 and the fourth lowest in the 72 years of record (USGS, 2016). Rainfall in parts of eastern Puerto Rico was more than 500 mm below normal over the first

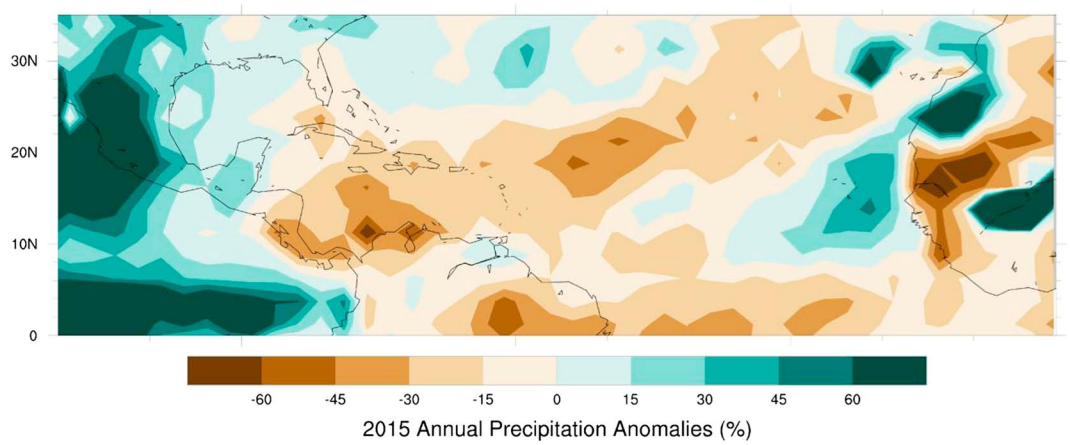

Figure 1. Percent precipitation anomaly for 2015 compared to a 1979–2014 climatology across the entire TNA. Anomalies were calculated using the Climate Prediction Center Merged Analysis of Precipitation data set (Xie & Arkin, 1997).

half of 2015, and April–July 2015 was the driest such 4 month period at the San Juan International Airport during the period of record, beginning in 1956 (NOAA NCEI, 2015). In the twentieth century, other major droughts affected the island in 1966–1968, 1971–1974, 1976–1977, and 1993–1995 (Larsen, 2000), with drought being recorded somewhere in Puerto Rico every 10 years; 15 consecutive days without rainfall occur roughly once every 15 years in the lower Luquillo Mountains (Scatena, 1995).

Though the 2015 drought was felt across nearly the entire Caribbean Basin (Figure 1), the impacts in Puerto Rico were both socially and ecologically unique compared to other droughts in the last 60 years in that they were harshest over the most densely populated and biologically diverse region of the island. Eastern Puerto Rico contains both the 2.35-million-person San Juan metropolitan area, claiming more than two thirds of the island residents, and the Luquillo Mountains and El Yunque National Forest, the only tropical rainforest in the U.S. National Forest system. In this high-biodiversity setting, droughts have widespread and lasting impacts on the ecosystems (Beard et al., 2005; Covich et al., 2003; Heartsill-Scalley et al., 2007). For example, fine-root biomass in the forest can take several years to recover, trees show increased investment in reproductive parts such as flowers and fruits (Beard et al., 2005), headwater riffles can dry out limiting access to microhabitats by benthic invertebrates (Covich et al., 2003), and long-term declines in amphibians (Burrowes et al., 2004) are enhanced during drought.

1.1. Rainfall Controls in the Eastern Caribbean

The scientific literature indicates competing schools of thought on El Niño/Southern Oscillation (ENSO) effects on precipitation in the Caribbean. ENSO warm phases have been shown to be associated with drought in Central America and parts of the Caribbean during July to October (e.g., Ropelewski & Halpert, 1987) with sea surface temperatures (SSTs) forming the basis of several effects, as described by Wu and Kirtman (2011), Jury and Gouirand (2011), and Gouirand et al. (2012). For example, Glenn et al. (2015) found that higher SSTs in the Atlantic Warm Pool are associated with increased rainfall during the late rainfall season (LRS, August–November) but did not identify a link with the early rainfall season (ERS, April–July). Taylor et al. (2011) demonstrated the role of a SST-driven geopotential gradient between the eastern tropical Pacific and tropical North Atlantic (TNA) in controlling Caribbean rainfall. Additionally, interannual SST variability within the TNA's main development region (MDR) for tropical waves is correlated with Caribbean rainfall, but the influence declines in the LRS when SSTs in the eastern tropical Pacific become more significant (Taylor et al., 2002).

In a comprehensive review of climatic hazards in the Caribbean Basin, Gamble (2014) noted that ENSO events are associated with decreased late summer and fall rainfall due to strong vertical wind shear over the TNA (Taylor et al., 2002) and lower frequency of hurricanes (e.g., Patricola et al., 2016; Ropelewski & Halpert, 1987, 1996). However, Gamble (2014) also noted that recent research has indicated more variability of the impact in the ENSO within the Caribbean Basin. As such, Malmgren et al. (1998) and Jury et al. (2007)

found no significant association between ENSO and rainfall for Puerto Rico and the lesser Antilles, while Chen and Taylor (2002) found that an influence on precipitation in the ERS was lagged to year +1 of the ENSO event. Meanwhile, the North Atlantic Oscillation (NAO) has a greater correlation with rainfall in the southeast Caribbean (e.g., Giannini et al., 2001; Jury et al., 2007). Nevertheless, national media (e.g., Alvarez, 2015) and federal agencies (e.g., USDA, 2015) in summer 2015 attributed the drought in eastern Puerto Rico directly to the strong ENSO warm event that was underway.

Another influence on rainfall in Puerto Rico is the Saharan Air Layer (SAL). The SAL is a mass of dry, dust-rich air that forms over the Sahara during the late spring to early fall and extends over the TNA as far west as North America. A feature of the tropical Atlantic above the trade wind moist layer, the SAL principally occupies the layer between 600 and 800 hPa with a distinctive easterly jet maxima around 650 hPa (Carlson & Prospero, 1972). The SAL is most active, characterized by larger outbreaks that reach farther west, from mid-June to late July, when it constitutes 40% of all Caribbean soundings. Tropospheric soundings during SAL events are 50–60% drier than a typical moist tropical sounding between 700 and 500 hPa and have ~20% less total precipitable water (Dunion, 2011). The SAL often transports high concentrations of mineral dust originating in Africa. North Africa is estimated to emit about 800 Tg yr^{-1} of dust each year (Huneeus et al., 2011); a large fraction of these emissions is carried to the west over the Atlantic Ocean, and they are often visible in satellite images in plumes from Africa into the Caribbean Basin (Prospero & Mayol-Bracero, 2013). Main source regions for aerosols in Puerto Rico during the recent DUST Aging and Transport from Africa to the Caribbean (Dust-ATTACk) intensive field campaign were found in the Western Sahara, Mauritania, Algeria, Niger, and Mali (Denjean et al., 2016). Aerosols in the SAL may inhibit convective cloud development and rainfall via microphysical processes (e.g., Albrecht, 1989; Dagan & Chemke, 2016; Dagan et al., 2015a, 2015b; Khain, 2009) while enhancing the trade wind inversion thereby limiting rainfall through thermodynamic and radiative effects (Rosenfeld et al., 2001).

Dunion (2011) created composite soundings for the Caribbean for maritime tropical air masses, midlatitude dry air intrusions, and SAL occurrence, and he noted that the mid-June to early August peak in SAL corresponded with precipitation patterns discussed in Hastenrath (1967) and termed the midsummer drought by Maganã et al. (1999). Angeles et al. (2010) demonstrated the role of the Saharan aerosols and associated changes in vertical wind shear on the midsummer dry period (or midsummer "drought"), which separates the ERS and LRS in July. While this relationship was strong in Barbados, it was not present in La Parguera, located in southwestern Puerto Rico.

Jury and Santiago (2010) demonstrated the multivariate nature of this link between Caribbean rainfall and African dust. In their examination of the impact of dust on the main development region for Atlantic hurricanes, they noted that cloud efficiency drops and the lapse rate stabilizes as aerosols increase. Critically, they found that increased dust reduces the development of Atlantic easterly waves via both advective and thermodynamic processes, while an anticyclone off the northwest coast of Africa increases upwelling. They also found that the warm, dry, subsiding air occurs with the African dust plume into the subtropics (18°N to 30°N) of the Atlantic. This work will explicitly examine the role of the warm, dry, subsiding air coincident with African dust on the drought in eastern Puerto Rico through the use of a new metric designed to examine atmospheric stability in the Caribbean.

1.2. Objective

Though a regular feature of Caribbean circulation patterns, the work presented here seeks to investigate the SAL's potential as a drought-causing mechanism by considering the 2015 eastern Puerto Rico event and to place the drought in context within the recent historical record. The Daymet 1 km daily rainfall product is used to assess the timing and magnitude of the drought in the complex topography of eastern Puerto Rico. Additionally, the experimental Gálvez-Davison Index (GDI) (Gálvez & Davison, 2016) is used to understand the impact of SAL intrusions on rainfall. This index has been used in the operational community to forecast convective rainfall in Puerto Rico, and components of the index are well suited to capture the effect of the hot, dry air intrusions above the trade wind inversion. We believe that this study presents the first application of the GDI to examine the impact of the SAL on rainfall at the monthly to seasonal scale. Additionally, we examine aerosol concentrations using sensors on the EOS-Aura and NOAA satellites and in situ observations from Cape San Juan.

2. Data and Methods

2.1. Daymet

The Oak Ridge National Laboratory Daymet v.3 data set provides gridded estimates of daily weather parameters for North America, including daily continuous surfaces of minimum and maximum temperature, rainfall occurrence and amount, humidity, shortwave radiation, snow water equivalent, and day length (Thornton et al., 2017). The gridded products are distributed at 1 km × 1 km spatial resolution for 1 January 1980 to 31 December 2016.

All station weather inputs were available from a single source, the NOAA National Centers for Environmental Information's Global Historical Climatology Network-Daily (GHCN-Daily) (Thornton et al., 2017). The current data set is based on the Thornton et al. (1997) methodology, which is designed to produce spatially continuous gridded products over large regions of complex terrain, which makes it well suited for examining rainfall in eastern Puerto Rico. Although the Daymet product has been available for the contiguous U.S. for several years, the Puerto Rico domain was released in 2016, and this is one of the first applications of the product for the island. The Daymet method is based on the spatial convolution of a truncated Gaussian weighting filter with the set of station locations, where sensitivity to the heterogeneous distribution of stations is accomplished with an iterative station density algorithm (Thornton et al., 1997). A daily rainfall occurrence is first calculated prior to the prediction of daily rainfall amount. Thornton et al. (1997) reported that a mean absolute error for predicted annual total rainfall was 19.3% of the observed annual totals and a success rate for predictions of rainfall occurrence of 83.3%. Daymet was used to examine the spatial distribution of daily rainfall in eastern Puerto Rico during 2015 and the most comparable drought year in the modern record, 1994.

2.2. Experimental Gálvez-Davison Index

The GDI is a stability index developed for tropical and subtropical locations that provides a measure of moist convective potential (Gálvez & Davison, 2014a, 2016). The GDI was developed to improve the prediction of shallower types of moist convection in the tropics to improve forecasts of tropical convection, particularly in the Caribbean. Common stability indices fail to adequately capture subsidence inversions and effects of upper level troughs and ridges in modulating convection (Gálvez & Davison, 2014a, 2016). The GDI uses temperature and mixing ratio at 950, 850, 700, and 500 hPa. Their methodology starts with the calculation of proxies for equivalent potential temperature within three layers to produce the column buoyancy index (CBI). A midlevel warming index (MWI) accounts for changes in midlevel stability from a warm ridge or a cool trough, and an inversion index (II) is calculated as trade wind inversions play an important role in inhibiting tropical convection (Gálvez & Davison, 2014b). The GDI is regularly used by the forecasters at the National Weather Service Forecast Office in San Juan, PR, as evidenced by frequent inclusion in their written forecast discussions.

Daily 18 UTC ERA-Interim reanalysis data were used to calculate GDI (Dee et al., 2011) as well as the 00 and 12 UTC radiosonde observations from the San Juan, PR (TJSJ). The GDI calculations from the two sources were well correlated ($R^2 = 0.74$), although the average GDI from radiosonde was greater than the reanalysis GDI by roughly 3.9 units. The reanalysis GDI was used for the remainder of this study due to temporal completeness and the availability of 18 UTC observations, which are closer to the 1500 LST (1900 UTC) peak in diurnal convective activity documented by Jury (2012).

The findings presented here are a unique use of the GDI to document SAL intrusions to eastern Puerto Rico. GDI and its components were calculated and aggregated for Puerto Rico east of 66.5°W, which includes all areas east of the highest peaks on the island in the Cordillera Central.

2.3. Aerosols

Goudie and Middleton (2001) and Prospero et al. (2002), among others, have shown that North Africa is the largest dust source in the world. Aerosols from North Africa are related to the NAO, the Madden-Julian Oscillation, and sea surface temperatures (e.g., Evan et al., 2008; Ginoux et al., 2004; Guo et al., 2013; Wong et al., 2008). As part of the Rain In Cumulus clouds over the Ocean-Puerto Rico Aerosol and Cloud Study (RICO-PRACS) campaign in 2004, an aerosol monitoring system was deployed at the Cape San Juan Observatory (18.38°N, 65.62°W, 66 m above sea level) on the northeastern coast of Puerto Rico. The station

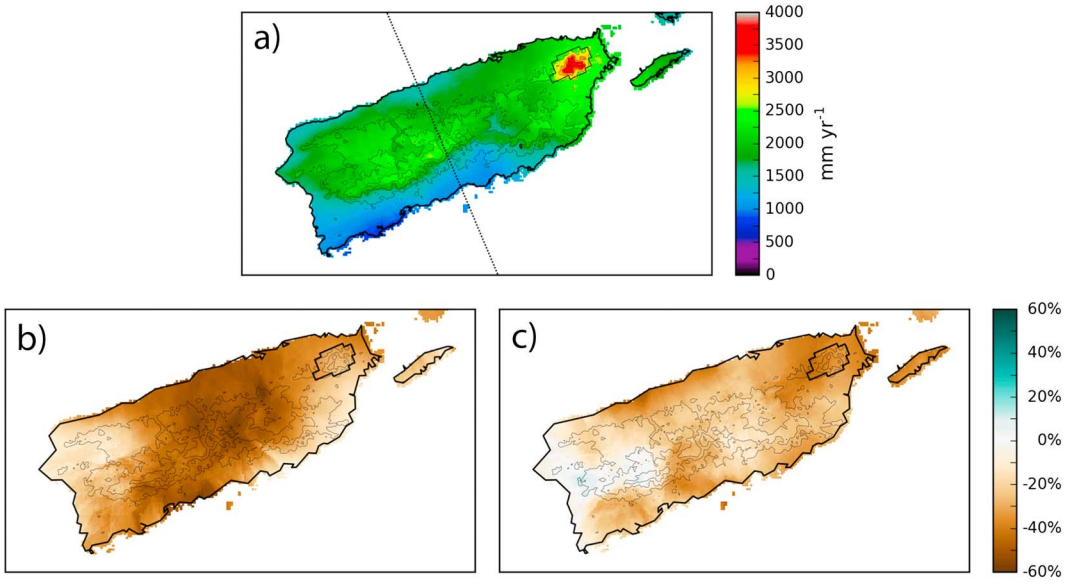

Figure 2. Comparisons of notable drought years to 30 year climatology (1985–2014) from Daymet. The (a) mean annual rainfall (mm) and percent rainfall anomalies for the years (b) 1994 and (c) 2015. El Yunque National Forest is outlined by a bold black line with the thin black lines representing 200, 500, and 800 m elevation contours. The dashed line in Figure 2a corresponds to the 66.5°W meridian.

is a regional Global Atmosphere Watch site and contributes to the National Oceanic and Atmospheric Administration-Earth System Research Laboratory (NOAA-ESRL, www.esrl.noaa.gov/gmd/aero/net/cpr/index.html) aerosol network and the NASA Aerosol Robotic Network (AERONET, http://aeronet.gsfc.nasa.gov/). Several spectral and derived products are available from AERONET, but this study focused on the aerosol optical thickness (AOT). AOT level 2 data are available at AERONET since 2005, although fewer than half of the years have consistent data reporting in April and May, whereas continuous data are available in June and July in nearly every year.

The European Centre for Medium-Range Weather Forecasting (ECMWF) Monitoring Atmospheric Composition and Climate (MACC) reanalyses resolve fields for chemically reactive and greenhouse gases and aerosols (Inness et al., 2013). The dust aerosol mixing ratio, the ratio of dust aerosol mass to the mass of its encompassing air, for particulates between 0.55 and 0.90 μm at 700 hPa was leveraged to gain a larger, spatially continuous perspective of aerosol transport from North African source to the Caribbean. Supplementing the reanalysis fields, observations from the Ozone Monitoring Instrument (OMI) on NASA's EOS Aura satellite were also examined. The OMI has been used to track dust transport globally, including African dust across the Atlantic (e.g., Denjean et al., 2016; Schepanski et al., 2012). The aerosol index (AI) is calculated based on the difference between the amount of ultraviolet (UV) light that the dust-filled atmosphere scatters compared to the amount of UV the atmosphere would backscatter without dust. See Torres et al. (2007) for the complete AI calculation. Values and anomalies for the MACC aerosol mixing ratio and the Aura OMI AI on a daily and monthly basis were examined in this study.

The AERONET data from Cape San Juan, Aura OMI, and ECMWF-MACC were used to examine the 2015 drought, but those products are only available for the most recent part of the precipitation record. The advanced very high resolution radiometer (AVHRR) AOT at a nominal 100 km resolution (AERO100) product was included to provide a longer time series beginning with the NOAA 15 satellite (June 1998 to December 2012). The data are provided as 1° latitude by 1° longitude global maps of AOT over the oceans. They are 1 week averages created from AVHRR channel 1 optical thickness retrievals from AVHRR global area coverage (4 km) data (Rao et al., 1989).

2.4. Analysis

The Daymet data were summed to monthly and annual averages and used to compare the magnitude, timing, and spatial distribution of rainfall anomalies in 2015 to the period of record, with attention given to the

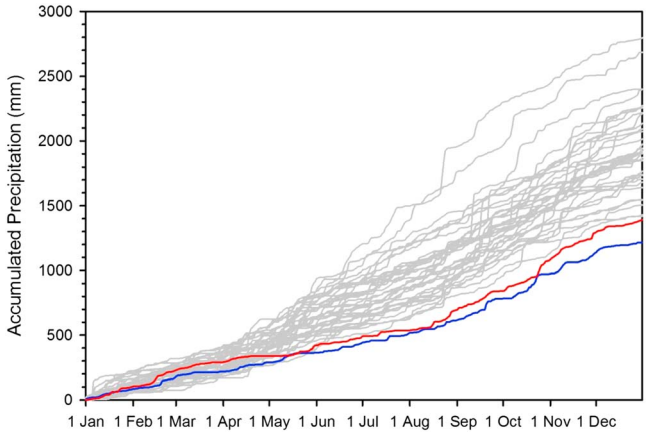

Figure 3. Cumulative annual rainfall total for the 36 year period 1980–2015 with 1994 (blue) and 2015 (red) bolded and colored from Daymet. Each trace represents the mean accumulated rainfall of eastern mainland Puerto Rico (east of 66.5°W) for a single year. The separation between the 2015 and 1994 traces that exists on 1 April disappears by mid-May when 2015 becomes briefly drier than 1994. This period represents the traditional ERS.

1994 drought. The GDI and the individual terms of the GDI were calculated daily from the ERA-Interim reanalysis over the eastern portion of Puerto Rico. These values were averaged on a weekly and monthly basis during the ERS for evidence of midlevel drying, an enhanced trade wind inversion, and other factors that would inhibit convection. As evidence of the role of the SAL, the aerosol time series from Cape San Juan was examined for the early rainfall season, augmented by weekly and monthly anomaly fields calculated from the ECMWF MACC aerosol dust mixing ratio and the Aura OMI AI. The aerosol data were examined for anomalously high values (>50% AI anomaly corresponding to roughly 0.6×10^{-7} MACC dust aerosol mixing ratio) in the early rainfall season and values that are consistent with the presence of the SAL.

3. Results

3.1. Overview of Drought Characteristics

The temporal and spatial variability of the 2015 drought in Puerto Rico is underscored by the Daymet daily gridded rainfall estimates. Compared to a 30 year climatology (1985–2014), Figure 2 shows that rainfall deficits over parts of eastern Puerto Rico approached 45% with some of the largest negative anomalies located in El Yunque National Forest. In contrast, parts of western Puerto Rico experienced slight positive rainfall anomalies with most positive anomalies smaller than 10% (maximum of 12.8%). Although the 1994 drought was characterized by greater rainfall deficits island wide, the San Juan metropolitan area and El Yunque National Forest in eastern Puerto Rico witnessed a more severe rainfall shortage in 2015. Rainfall anomalies in El Yunque were approximately 10% more negative in 2015 compared to 1994.

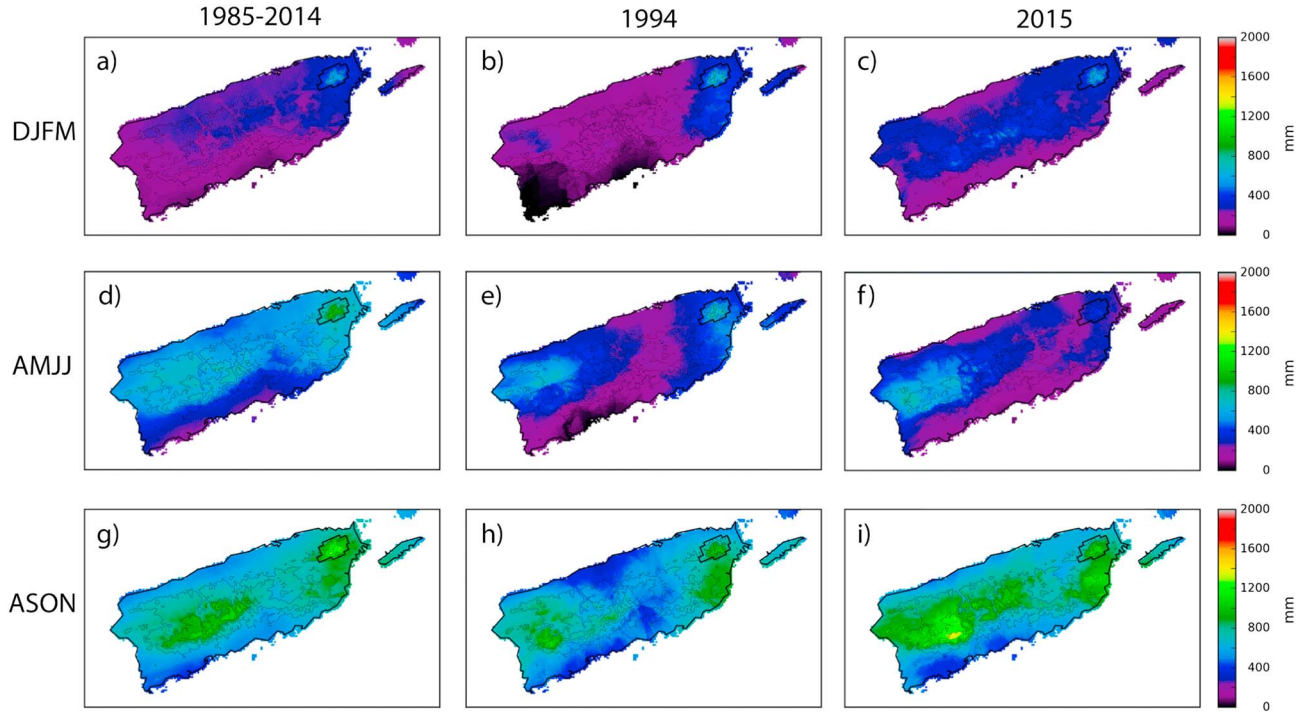

Figure 4. Seasonal rainfall totals for notable drought years (b, e, and h) 1994 and (c, f, and i) 2015 compared to the (a, d, and g) 1985–2014 30 year climatology from Daymet. Rainfall totals are calculated for the dry season (December–March, Figures 4a–4c), ERS (April–July, Figures 4d–4f), and LRS (August–November, Figures 4g–4i).

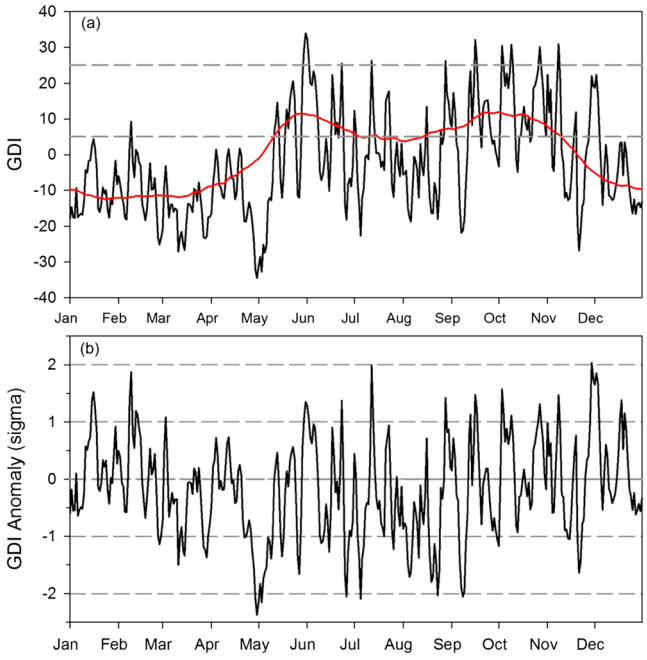

Figure 5. (a) Daily mean GDI averaged across eastern Puerto Rico (east of 66.5°W) for 2015 (black) and the 1979–2015 average (red). (b) Daily anomaly of GDI expressed in terms of standard deviations from the mean.

In addition to the spatial variation in drought severity, the Daymet data set helps establish the periods of most significant rainfall departures. Figure 3 shows that through the end of March, the mean cumulative rainfall across eastern Puerto Rico (east of 66.5°W) was near the 1980–2015 average. Despite the normal start to the year, by mid-May the 2015 average total rainfall deficit across eastern Puerto Rico surpassed 1994 in severity, and through mid-August, the 2015 and 1994 droughts remained roughly equivalent over the eastern half of the island.

This seasonal and spatial component to the 2015 drought development is also captured in Figure 4. Caribbean rainfall season is largely bimodal with relative maxima during the ERS and LRS (e.g., Van Beusekom et al., 2015). Whereas late 2014 and early 2015 experienced slightly above average rainfall (Figure 4c), especially compared to 1994 (Figure 4b), the early rainfall season was exceptionally dry (Figure 4f) for eastern Puerto Rico. This region of the island registered an average of 246.1 mm of rainfall during this 4 month span. This represents a −61.8% departure from the 1985–2014 early rainfall season mean of 644.5 mm, a value exceeding the −54.5% anomaly experienced by this same area during the 1994 drought. Sorely needed rainfall in late 2015 (Figures 3 and 4) helped temper the year's final rainfall totals when compared to 1994, masking the signature of the unprecedented midyear drought. Though 2015 was generally unfavorable for tropical cyclone activity in the Caribbean and western Atlantic, Hurricane Danny and Tropical Storm Erika brought needed relief to the drought in late August, although Erika also caused $17.4 million in damage and left 200,000 without power (Pasch & Penny, 2016; Stewart, 2016).

3.2. Thermodynamic and Synoptic Signature of the SAL

Previous work has examined the SAL using common stability indices for the midlatitudes, such as convective available potential energy, convective inhibition, the *K* index, or lifted index (e.g., Dunion, 2011). However, these stability indices have shortcomings in the tropics due to differences in the physical processes associated with convection in the midlatitudes and tropics (e.g., Ramage, 1995). The GDI was used to determine the role of changes in atmospheric stability, particularly midtropospheric warming and enhanced stability that would be a signature of the SAL in the tropics. A time series of daily average GDI was calculated for 2015 averaged over eastern Puerto Rico, and average GDI was calculated each week of the year over the ERA-Interim record (1979–2015). The GDI reached a minimum each January and February, near a value of −10, which corresponds to a strong subsidence inversion (Figure 5a and Table 1). The maximum GDI is typically in late May and early June, and again in late September and early October, when values exceed 10 on average, but days exceeding 25 are not uncommon even in a drier than average year (Figure 5a). The values presented in Table 1 were predicated on single observations, while Figure 5a shows averages over space.

Table 1
Critical GDI Values and Convection Type (NOAA WPC, 2016)

GDI	Expected convective regime
> +45	Scattered to widespread thunderstorms
+35 to +45	Scattered thunderstorms and/or widespread shallow convection
+25 to +35	Scattered shallow convection and isolated to scattered thunderstorms
+15 to +25	Isolated to scattered shallow convection and a few isolated thunderstorms
+5 to +15	Isolated to scattered shallow convection; any thunderstorm brief and isolated
−20 to +5	Isolated to scattered shallow convection; strong subsidence inversion likely
< −20	Fair conditions; any convection should be shallow, isolated, and produce light rain

Note. These categories differ slightly from the most recent suggestions by Gálvez and Davison (2016) but better characterize the GDI climatology of the study area.

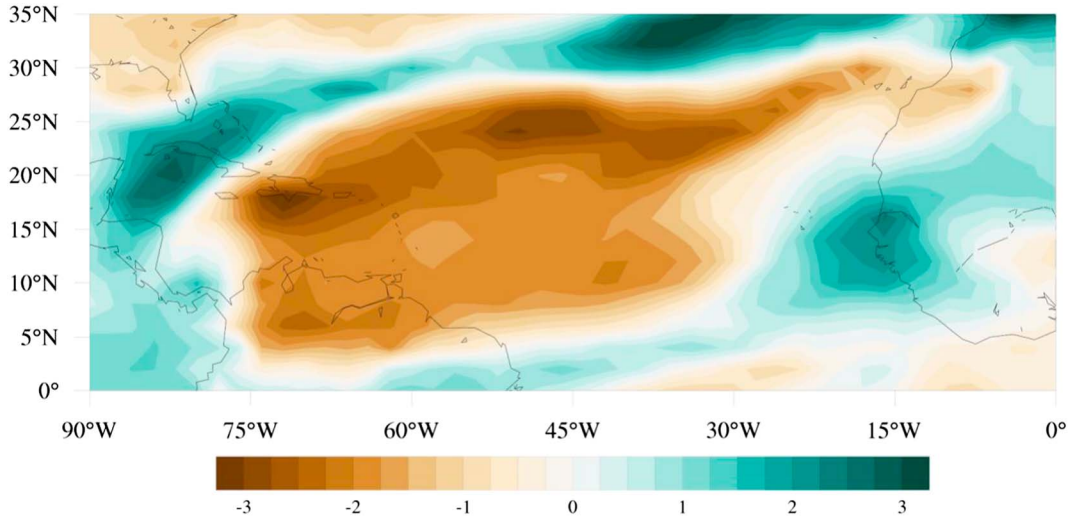

Figure 6. Weekly GDI departure from average expressed in standard deviations for the week of 30 April 2015 to 6 May 2015. Brown (green) contours represent lower (higher) than climatological GDI. This temporally aligns with record temperatures observed in Venezuela.

During 2015, prolonged periods of below average GDI occurred from March until mid-August, only briefly punctuated by periods with GDI above the average, most notably in early June (Figure 5a). Throughout late April and early May 2015, the GDI often approached 2 standard deviations below the mean (Figure 5b), indicating conditions much less conducive to thunderstorm development and rainfall than typical for that time of year.

Analysis of weekly GDI anomalies across the TNA and Caribbean Sea indicated near-normal convective potential during January and February. At the end of April, an area of strong negative GDI anomalies was observed over the eastern Caribbean and South America (Figure 6). The departures from average were expressed in terms of standard deviations to illustrate the significance of these differences and to standardize across the spatial domain of the maps. This area of enhanced stability advected west and south during the following week (not shown). Analysis of the GDI anomalies suggests that the eastern Puerto Rico drought was at least in part due to decreased convective potential extending across multiple scales of motion. While negative GDI anomalies were strong in the eastern Caribbean, negative anomalies were also present throughout the TNA. Thus, easterly wave development in the MDR was slowed in addition to the decrease in trade wind convection in the eastern Caribbean, which may have inhibited tropical storm formation. For example, Dunion and Velden (2004) found that when the SAL engulfs tropical waves, tropical disturbances, or preexisting tropical cyclones, its dry air, inversion, and strong vertical wind shear can inhibit the ability of tropical cyclones to strengthen. Furthermore, when tropical cyclones do produce rainfall in Puerto Rico, the rainfall amount is closely related to the total precipitable water (Hernández Ayala & Matyas, 2016). Thus, reduced rainfall in Puerto Rico can be attributed to a lack of localized rainfall in addition to a lower frequency of organized, mesoscale tropical systems across the TNA and Caribbean.

The component terms of the GDI, described in section 2.2, were also investigated to infer the atmospheric processes responsible for the decreased convective potential across the study area. The II term, related to the trade wind inversion (TWI) intensity, is a measure of stability across the inversion and dry air entrainment. Analysis of the II term during 2015 indicates strong negative anomalies over the study region beginning in March. These negative anomalies were associated with a stronger inversion when compared to the climatological strength of the TWI. The most negative II departures were observed during 30 April to 6 May 2015 and were greater than 3 standard deviations below the average. As with the GDI and MWI terms (not shown), these negative departures persisted and resulted in II values much below normal for all of April (Figure 7a) and May 2015 (Figure 7b). In addition to the anomalous inversion, the weekly anomalies in the MWI term suggest that periodic increased midlevel warming occurred across the Caribbean and TNA throughout early rainfall season.

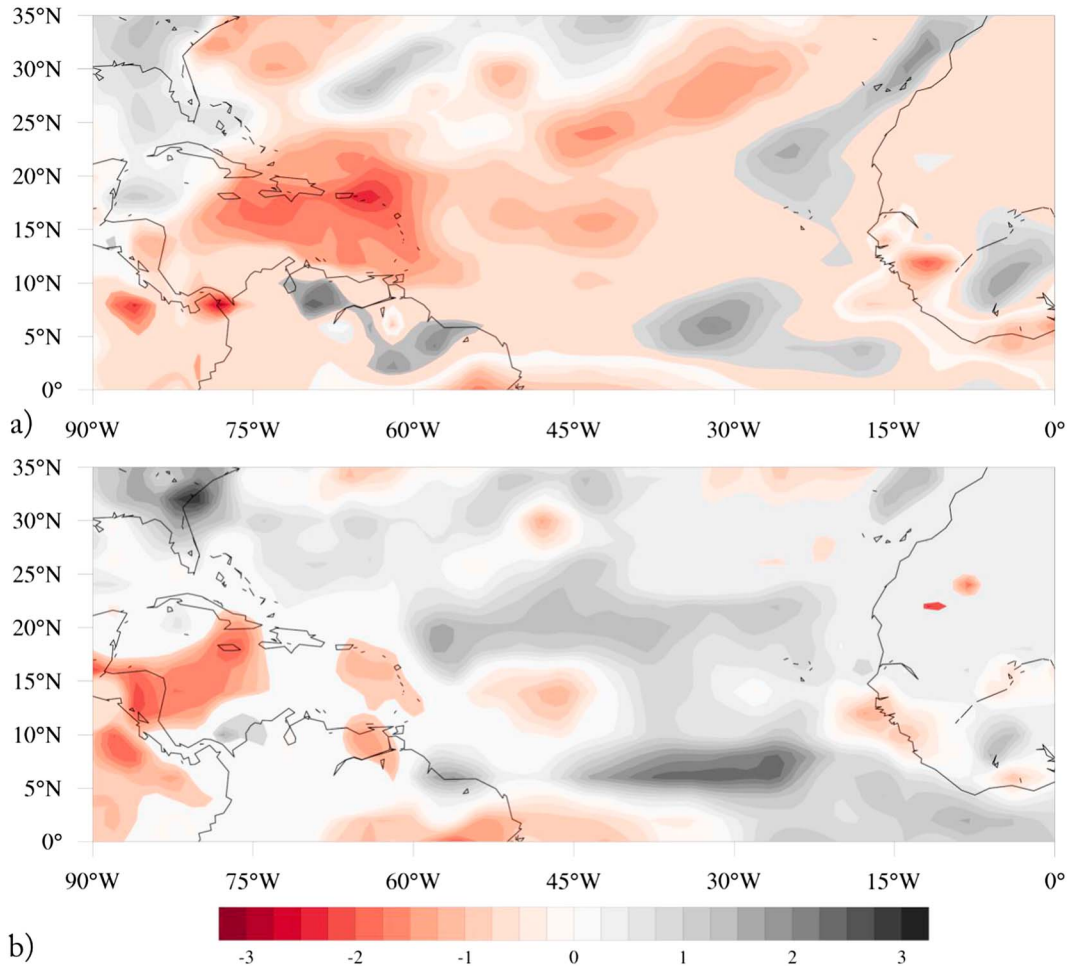

Figure 7. (a) April and (b) May 2015 departure from average expressed in standard deviations for the II term. Red (gray) contours represent a stronger (weaker) inversion compared to the monthly climatology.

The relationship between GDI, NAO, and ERS rainfall was also examined for the period of 1980–2015. GDI and eastern Puerto Rico rainfall were calculated as described above and plotted with ENSO warm events as determined from the Nino3.4 sea surface temperature (SST) anomalies. A clear relationship was evident between ERS rainfall anomalies; years with average GDI of less than 2.4 were associated with below average rainfall, while those with GDI greater than 2.4 were associated with above average rainfall in the ERS (Figure 8a). A scatterplot of GDI and rainfall anomalies during the ERS shows a strong correlation (R^2 = 0.64), while there appears to be little relationship between ENSO warm and cold events and ERS rainfall anomalies in eastern Puerto Rico (Figure 8b). As the MWI term is calculated from a level (500 hPa) that often is above the SAL over the Caribbean (see Figure 2 in Braun, 2010), the II and CBI terms were examined independent of the GDI. The sum of these two components of the GDI has an even stronger relationship (R^2 = 0.71) with the ERS rainfall over eastern Puerto Rico, highlighting the importance of these two terms, which are both strongly affected by the SAL. AVHRR AOT from the AERO100 product was also compared to the ERS rainfall anomalies for eastern Puerto Rico since 1999. The AERO100 product is only available over the ocean; therefore, the AOT values were averaged over region of primary transport to Puerto Rico from the adjacent Caribbean Sea to the south of and surrounding Puerto Rico (65°–80°W, 10°–20°N), roughly corresponding to the spring and summer transport routes shown in Meng et al. (2017). A scatterplot of AOT and rainfall anomalies shows a significant correlation (R^2 = 0.47), albeit not as robust as the relationship with GDI (Figure 8c). Additional discussion of the role of aerosols is presented in section 3.3.

The role of ENSO in the Caribbean previously has been examined in conjunction with the role of the NAO (e.g., Jury et al., 2007; Malmgren et al., 1998). Here the average monthly NAO from the NOAA Climate

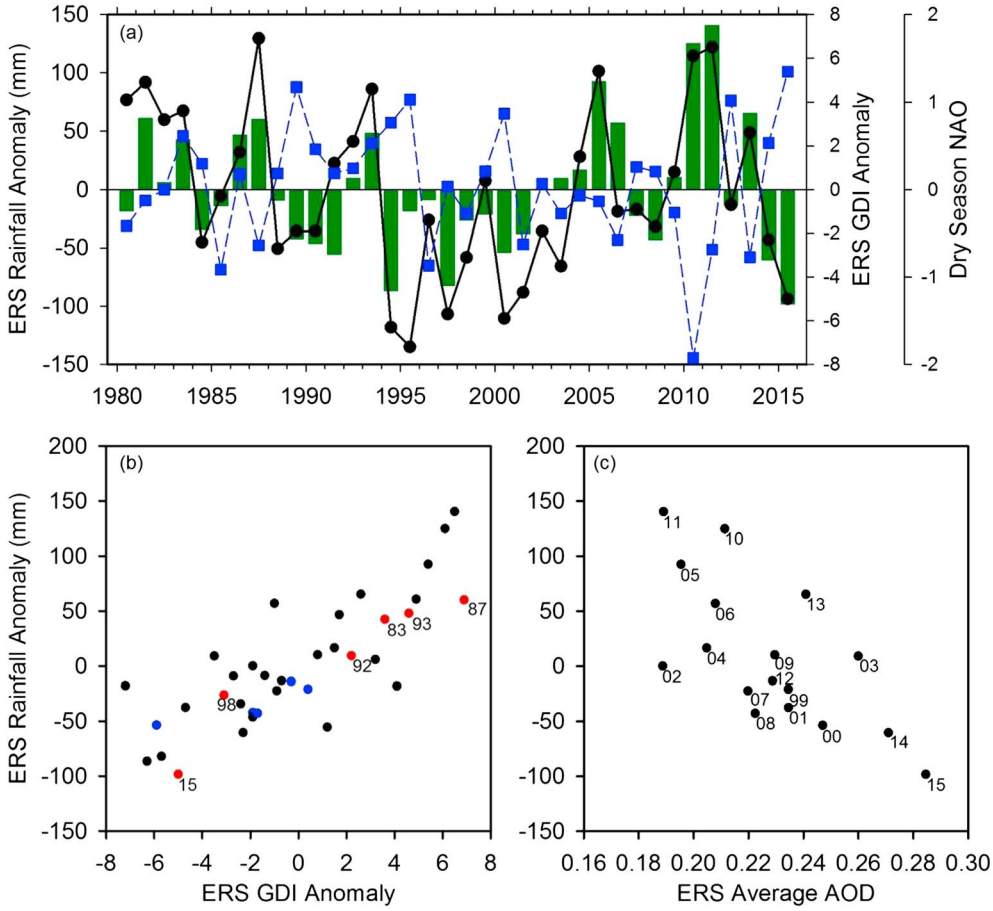

Figure 8. (a) Early rainfall season (ERS) rainfall anomalies (green bars), GDI anomalies (solid black line and circles), and average NAO during the preceding dry season (December-January-February-March) (dashed blue line and squares). (b) GDI anomalies versus rainfall anomalies during the ERS for the same period showing years with ENSO warm (red, years labeled) and cold (blue) events colored. Black dots represent years with Nino3.4 departures less than ±0.5°C. (c) AVHRR AOT from the NOAA AERO100 product for the adjacent Caribbean Sea versus rainfall anomalies during the ERS (years labeled).

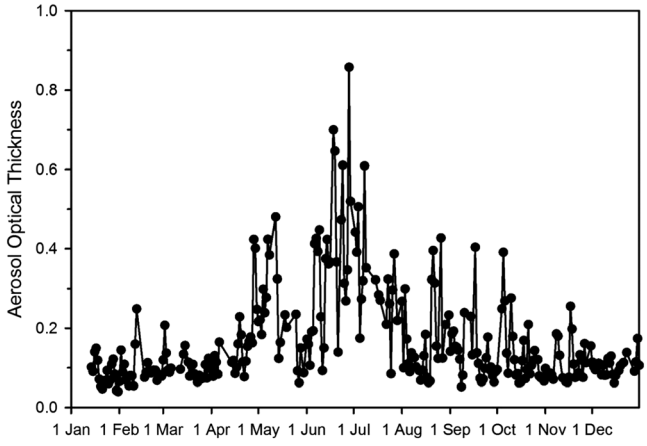

Figure 9. Aerosol optical thickness (AOT) at 440 nm from the Cape San Juan Observatory for 2015.

Prediction Center, based on the methodology of Barnston and Livezey (1987), was compared to the ERS rainfall anomalies. The time series were inversely correlated (R^2 = 0.35), with a positive phase of the NAO during the dry season associated with decreased ERS rainfall (Figure 8a). This is consistent with the findings by Malmgren et al. (1998) of decreased annual rainfall associated with a positive winter NAO and the findings by Jury et al. (2007) that winter NAO is negatively correlated with the spring rainfall in Lesser Antilles and eastern Puerto Rico. The positive phase of the NAO is associated with an enhanced North Atlantic Subtropical High, a stronger trade wind inversion, and stronger nearsurface winds (i.e., the Caribbean low-level Jet). This also may contribute to the SAL reaching eastern Puerto Rico earlier in the season.

3.3. SAL Evidence in Aerosols

The GDI and its components, particularly the II, illustrate the increased prevalence and persistence of a more stable environment with increased hot, dry air associated with the TWI. Nevertheless, the GDI does not directly indicate the presence of the SAL. To provide

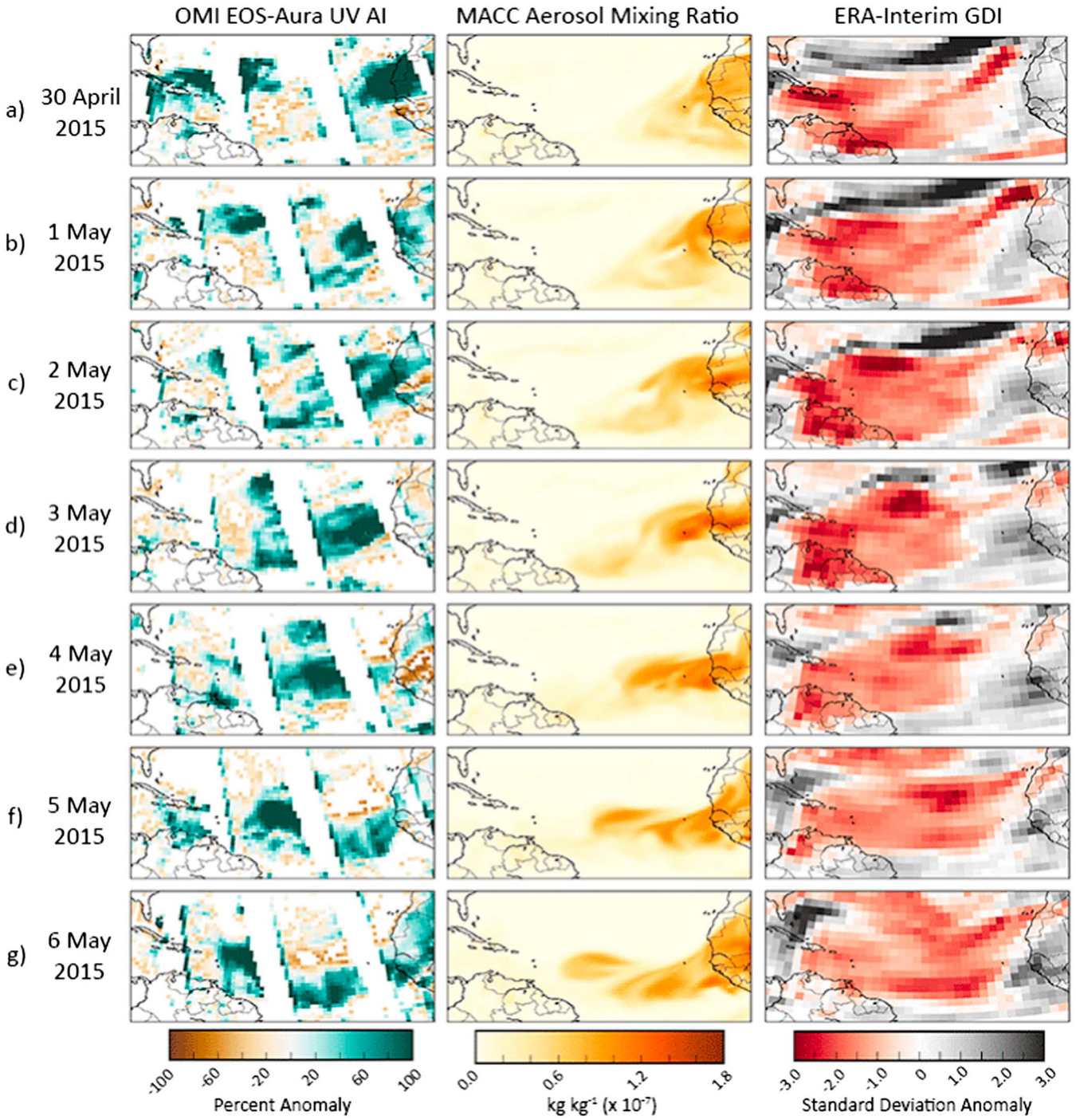

Figure 10. (a–g) Time series of 30 April to 6 May 2015 SAL outbreak. OMI EOS-Aura UV aerosol index daily anomalies (left) are presented beside ECMWF/MACC model analyses of the 0.55–0.90 μm aerosol mixing ratio at 700 hPa (middle) and GDI II departures from the 1979–2015 climatology (right). Daily AI anomalies were computed against the 2005–2016 monthly April and May mean, respectively. The large concentration of aerosols depicted above roughly coincides with the relative maximum of AOT detected during May 2015 (Figure 9).

additional evidence of the intrusion of air masses of Saharan origin, in situ aerosol data from Cape San Juan were examined for 2015 (Figure 9). AOT data at 440 nm indicate an increase from values of approximately 0.1 to 0.4 in late April and early May. By comparison, during the Puerto Rico Dust Experiment (PRIDE), midvisible (440–870 nm) AOT in Puerto Rico averaged 0.25, with a maximum >0.5 and with clean marine periods of

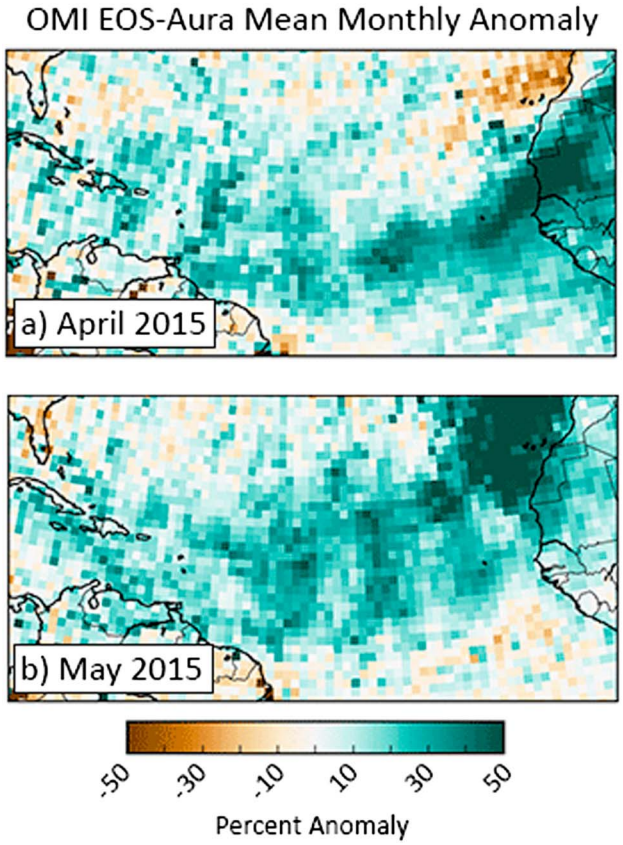

Figure 11. OMI EOS-Aura UV aerosol index mean monthly anomalies are depicted for April and May 2015. Mean monthly anomalies were computed using the 2005–2016 April and May climatologies, respectively.

approximately 0.08 (Reid et al., 2003). Mean AOT at 440 nm for May was greater than all but one other year of available data (2007), and mean AOT for April was also greater than all but one year (2010). The mean AOT combined for April and May was greater than the other six years with sufficient data to examine.

To confirm the findings with the AOT data from Cape San Juan, the ECMWF MACC reanalysis product was examined, which provides a dust aerosol mixing ratio. Further, remotely sensed observations were incorporated using aerosol index values measured by EOS-Aura OMI. Figure 10 depicts the coevolution of II reductions, OMI-observed AI, and MACC-resolved dust plume transit during 30 April to 6 May 2015. The pattern resembles the OMI-detected plumes in June–July 2012 described by Denjean et al. (2016). Because the SAL typically does not influence the Caribbean until mid-June and July, even seemingly minor aerosol loadings near Puerto Rico in late April and early May can represent significant departures from normal. Consequently, Figure 10 expresses OMI AI in terms of anomalies from the 12 year (2005–2016) period of record for the OMI satellite data, whereas the MACC-modeled images are depicted as true values to illustrate the spatially continuous evolution of the plumes. Figure 10a shows that large positive anomalies existed near Puerto Rico on 30 April with a swath of large AI anomalies persisting across the TNA for the next 6 days. Figure 11 provides greater context for the AI departures by showing mean monthly OMI AI anomalies for April (Figure 11a) and May 2015 (Figure 11b). The monthly OMI AI anomalies corroborate the results of the GDI analysis by showing that the SAL was persistently influencing convective potential well before its climatologically expected arrival in Puerto Rico.

To consider the impact of aerosols on early season rainfall in other years, one-point correlation maps of AVHRR aerosol optical thickness from the NOAA AERO100 product and eastern Puerto Rico precipitation were created for each month in the ERS and for the entire ERS (Figure 12). When large numbers of correlations are examined across a spatial domain (i.e., a "field"), a number of individual correlations may pass a test of significance by chance. A field significance test is important for evaluating the collective significance of a number of individual tests. A Monte Carlo approach proposed by Livezey and Chen (1983) is used here to assess the significance of the field, defined by the domain of 15°W to 85°W and 5°N to 25°N, using 10,000 simulations. The field significance tests indicate that the June result (Figure 12c) was significant at the 99% confidence interval, April (Figure 12a), May (Figure 12b), and the ERS results (Figure 12d) were significant at the 90% confidence interval. July (not shown) had few areas with significant correlations, and the field test was not significant.

The June and ERS results, which are most robust, show an area of high correlations in the Caribbean Sea, with the largest correlations coefficients ($|R| > 0.8$) immediately south of the island of Hispaniola and significant correlations extending to West Africa north of 5°N latitude (Figures 12c and 12d). The correlations extending to West Africa provide important evidence of the link to the source region. The highest correlations in the Caribbean Sea, to the southwest of Puerto Rico, correspond to the most common transport paths for aerosols shown by Huang et al. (2010) across the Lesser Antilles (see their Figures 1 and 6).

4. Discussion

The suppression of the early rainfall season was especially critical to establishing the 2015 drought in advance of the perennial midsummer dry spell (Gamble et al., 2008). As discussed in section 1, much previous drought control work in the Caribbean has focused on global and/or hemispheric modes of low-frequency climate variability. However, such research is hard-pressed to explain the 2015 rainfall anomaly. For instance, Giannini et al. (2000) found a positive correlation between spring and early summer Caribbean rainfall and

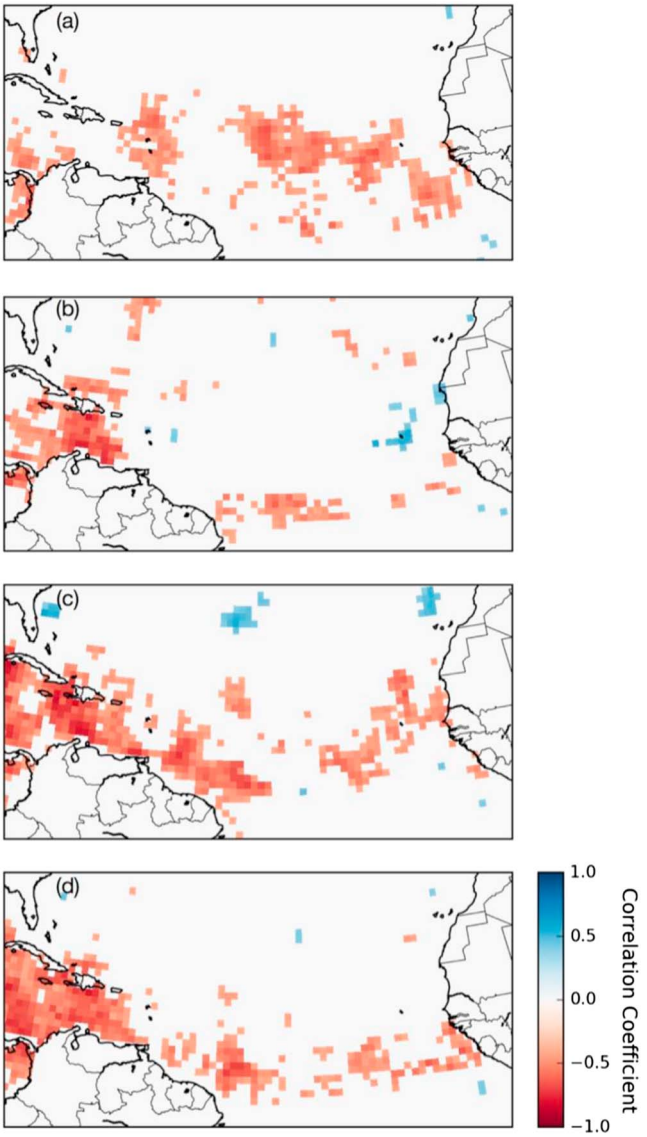

Figure 12. One-point correlation maps of AVHRR AOT from the NOAA AERO100 product and eastern Puerto Rico precipitation for (a) April, (b) May, (c) June, and (d) the early rainfall season (ERS) during 1999–2015. Only point correlations significant at 90% confidence interval ($|R| \geq$ than 0.40) are shown. Field significance tests indicate that the June result is significant at the 99% confidence interval, while April, May, and ERS results are significant at the 90% confidence interval.

ENSO warm events which is seemingly incongruous with the occurrence of the 2015 drought during the strong ENSO event. Further, Charlery et al. (2006) found that the influence of the NAO on eastern Caribbean rainfall is dependent on the phase and intensity of ENSO. Without a clear consensus regarding the roles of large-scale low-frequency modes of climate variability, the SAL poses a much more temporally and spatially targeted mechanism of eastern Caribbean drought, as exemplified during the 2015 early rainfall season. While the GDI calculation does not directly indicate the presence of the SAL, in conjunction with the increased aerosols during April and May, it provides strong evidence of the presence of Saharan air during this period. While the strong 2015 El Niño and positive NAO events may have contributed to the drought, the direct causal mechanism is more clearly associated with the SAL.

Our findings indicate that the SAL exerted a threefold influence through its (1) early arrival in the eastern Caribbean, (2) increased strength during its typical period of activity (as expressed by the GDI), and (3) prevalence extending beyond Puerto Rico to include regions of historical tropical cyclone development. The GDI was well below average throughout the early and late 2015 rainfall seasons with marked negative anomalies beginning in March, coincident with the Daymet-indicated drought onset. Though the SAL is a regular feature of the eastern Caribbean's middle-to-lower troposphere, the presence of the SAL-like air layer during the early rainfall season is exceptional. Pronounced negative anomalies of the GDI's II term, corresponding physically to stability and drying across the TWI, indicate that any cumulus towers would have struggled to penetrate the warm layer, preventing their growth into mature, precipitating convection. Exacerbating its early onset, the GDI anomalies indicate that the SAL maintained a stronger-than-average signal during the typical midsummer dry spell in 2015. Figure 5a illustrates that the mid-June through July period is climatologically associated with weaker GDI values; however, even during this annually less favorable period for convection, negative GDI anomalies greater than 1 standard deviation persisted. These findings are extensible beyond 2015. Key results presented here are the strong relationship between GDI and ERS rainfall anomalies in eastern Puerto Rico since 1980 (Figure 8), and the relationship between ERS, particularly June, precipitation and aerosols in the Caribbean Sea to West Africa since 1999 (Figure 12). The findings presented here indicate a relationship between an active SAL over the Caribbean and a reduction in rainfall during the ERS, but this relationship is not as clear in July, during the midsummer dry period. Notably, the II and CBI, which are the components of the GDI most associated with the increase in the TWI, showed the most robust relationship with ERS rainfall. However, it is important to note that the SAL and associated dust layer are not always contiguous. For example, Wong and Dessler (2005) suggested that dust is only a good proxy to track the SAL in the area close to the African continent. Furthermore, dust apparent in satellite imagery may persist over the Caribbean even after the thermodynamic structure of the SAL is no longer evident.

Beyond Puerto Rico, March 2015 GDI anomalies were negative across most of the Caribbean with anomalies as large as 3 standard deviations near the Bahamas. Additionally, negative GDI anomalies were present in the eastern hurricane MDR (10°–20°N, 80°–20°W). April GDI anomalies indicate decreased convection throughout most of the MDR with larger anomalies just outside of the MDR over the Sahel and Canary Islands. From May to September, negative anomalies persist throughout the eastern Caribbean. The results presented here indicate negative anomalies in the GDI across the Caribbean and upwind of Puerto Rico in the TNA. This effect is

indicative of suppressed convective potential both locally and in development regions for tropical waves that are typically rainfall-triggering mechanisms for Puerto Rico.

Though the 2015 Puerto Rico drought event has provided an illustration of the role of the SAL in drought production in the ERS, its potential as broader drought-influencing mechanism is also apparent. Furthermore, the 2015 drought event provides an example of future droughts which may become more frequent in response to anthropogenic climate change (Karmalkar et al., 2013). Climate models project drier conditions for the Caribbean through the end of the century. Most notably, the largest-magnitude decreases are expected to occur during the ERS (Karmalkar et al., 2013), which temporally aligns with the peak of the 2015 drought.

5. Conclusion

The 2015 Puerto Rico drought led to substantial impacts on infrastructure, water supply, and ecology. The largest rainfall deficits (roughly −45% anomalies) were experienced in eastern Puerto Rico and the Luquillo Mountains, adversely impacting the municipal water supply for the San Juan metropolitan area and the stream and forest ecology of the El Yunque National Forest. Climatologically, Puerto Rico exhibits a bimodal rainfall pattern with a dry season (December–March), followed by the ERS and LRS. Typically, in June and July, a decrease in rainfall leads to a midsummer dry period in the Caribbean. The 2015 rainfall deviated from the typical bimodal pattern due to a suppression of the ERS, resulting in a de facto extension of the midsummer dry period to encompass April–July. Rainfall anomalies during this 4 month span were approximately −62% across eastern Puerto Rico, a more severe deficit than the previous drought of record in 1994. The 1994 drought was also marked by GDI and II anomalies nearly as low as 2015, a positive NAO during the preceding dry season, and a severe dust event in June 1994 (Petit et al., 2005). Unfortunately, no satellite aerosol data are available for 1994, and no in situ measurements are available for Puerto Rico that year.

This work shows that the severe ERS dry period coincided with abnormally early and strong SAL activity in the Caribbean Basin. The thermodynamic signature of the SAL activity is inferred through anomalously low values of a newly established measure of moist convective potential, the Gálvez-Davison Index. Additionally, remotely sensed, modeled, and in situ data sources demonstrate that low GDI values were collocated with high dust concentrations in the Caribbean. A consistent pattern of ERS rainfall suppression is linked with increased atmospheric stability, an enhanced TWI, and higher dust concentrations, which are characteristic of the SAL.

Future work should attempt to better understand the relative role of thermodynamic versus cloud microphysical effects of the SAL on rainfall and the relative impact on local convection versus organized convection through easterly waves. Additional work should also focus on the pathways by which changes in large-scale circulation (e.g., NAO) and sea surface temperatures are linked to rainfall suppression during SAL outbreaks into the Caribbean, particularly during the ERS. The work presented here is perhaps the first to explicitly demonstrate a relationship between the SAL and rainfall during the early rainfall season, but this relationship is not as clear in July, during the midsummer dry period. Future work should focus more specifically on the role of the SAL during the midsummer dry period and during the transition to the late rainfall season.

Acknowledgments

We thank Olga Mayol-Bracero and her staff for establishing and maintaining the Cape San Juan NASA AERONET site used in this investigation. The authors thank Alan Covich, Doug Gamble, Andrew Grundstein, and J. Marshall Shepherd for their helpful comments on a draft of this manuscript. The authors also thank three anonymous reviewers for their many constructive comments. The AERO100 aerosol optical thickness data were accessed from the NOAA CLASS archive (https://www.class.ncdc.noaa.gov). ERA-Interim (http://apps.ecmwf.int/datasets/data/interim-full-daily) and ECMWF MACC reanalysis data (http://apps.ecmwf.int/datasets/data/macc-reanalysis) were accessed from the ECMWF archive. Aura OMI data were accessed from the NASA Giovanni archive (https://giovanni.gsfc.nasa.gov). Cape San Juan aerosol data were archived from the NASA AERONET archive (https://aeronet.gsfc.nasa.gov/). TSJS radiosonde data were accessed from the NOAA/ESRL radiosonde database (https://ruc.noaa.gov/raobs). All other data sets are listed in the references. This research was supported by the NSF Luquillo Long-Term Ecological Research Program (1239764) through a subaward from the University of Puerto Rico-Rio Piedras to the University of Georgia.

References

Albrecht, B. A. (1989). Aerosols, cloud microphysics, and fractional cloudiness. *Science*, *245*(4923), 1227–1230. https://doi.org/10.1126/science.245.4923.1227

Alvarez, L. (2015). Water crisis brings out Puerto Rico's creative side, accessed 2 April 2017. Retrieved from: http://www.nytimes.com/2015/07/15/us/in-drought-puerto-rico-rations-water-setting-off-a-collection-frenzy.html?_r=0

Angeles, M. E., González, J. E., Ramírez-Beltrán, N. D., Tepley, C. A., & Comarazamy, D. E. (2010). Origins of the Caribbean rainfall bimodal behavior. *Journal of Geophysical Research*, *115*, D11106. https://doi.org/10.1029/2009JD012990

Barnston, A. G., & Livezey, R. E. (1987). Classification, seasonality and persistence of low-frequency atmospheric circulation patterns. *Monthly Weather Review*, *115*(6), 1083–1126. https://doi.org/10.1175/1520-0493(1987)115%3C1083:CSAPOL%3E2.0.CO;2

Beard, K. H., Vogt, K. A., Vogt, D. J., Scatena, F. N., Covich, A. P., Sigurdardottir, R., … Crowl, T. A. (2005). Structural and functional responses of a subtropical forest to 10 years of hurricanes and droughts. *Ecological Monographs*, *75*(3), 345–361. https://doi.org/10.1890/04-1114

Braun, S. A. (2010). Reevaluating the role of the Saharan air layer in Atlantic tropical cyclogenesis and evolution. *Monthly Weather Review*, *138*(6), 2007–2037. https://doi.org/10.1175/2009MWR3135.1

Burrowes, P. A., Joglar, R. L., & Green, D. E. (2004). Potential causes for amphibian declines in Puerto Rico. *Herpetologica*, *60*(2), 141–154. https://doi.org/10.1655/03-50

Carlson, T. N., & Prospero, J. M. (1972). The large-scale movement of Saharan air outbreaks over the northern equatorial Atlantic. *Journal of Applied Meteorology*, *11*(2), 283–297. https://doi.org/10.1175/1520-0450(1972)011%3C0283:TLSMOS%3E2.0.CO;2

Charlery, J., Nurse, L., & Whitehall, K. (2006). Exploring the relationship between the North Atlantic Oscillation and rainfall patterns in Barbados. *International Journal of Climatology*, *26*(6), 819–827. https://doi.org/10.1002/joc.1334

Chen, A., & Taylor, M. A. (2002). Investigating the link between early season Caribbean rainfall and the El Niño +1 year. *International Journal of Climatology*, *22*(1), 87–106. https://doi.org/10.1002/joc.711

Covich, A., Crowl, T., & Scatena, F. (2003). Effects of extreme low flows on freshwater shrimps in a perennial tropical stream. *Freshwater Biology*, *48*(7), 1199–1206. https://doi.org/10.1046/j.1365-2427.2003.01093.x

Dagan, G., & Chemke, R. (2016). The effect of subtropical aerosol loading on equatorial precipitation. *Geophysical Research Letters*, *43*, 11,048–11,056. https://doi.org/10.1002/2016GL071206

Dagan, G., Koren, I., & Altaratz, O. (2015a). Competition between core and periphery-based processes in warm convective clouds—From invigoration to suppression. *Atmospheric Chemistry and Physics*, *15*(5), 2749–2760. https://doi.org/10.5194/acp-15-2749-2015

Dagan, G., Koren, I., & Altaratz, O. (2015b). Aerosol effects on the timing of warm rain processes. *Geophysical Research Letters*, *42*, 4590–4598. https://doi.org/10.1002/2015GL063839

Dee, D. P., Uppala, S. M., Simmons, A. J., Berrisford, P., Poli, P., Kobayashi, S., … Vitart, F. (2011). The ERA-Interim reanalysis: Configuration and performance of the data assimilation system. *Quarterly Journal of the Royal Meteorological Society*, *137*(656), 553–597. https://doi.org/10.1002/qj.828

Denjean, C., Formenti, P., Desboeufs, K., Chevaillier, S., Triquet, S., Maillé, M., … Ogren, J. (2016). Size distribution and optical properties of African mineral dust after intercontinental transport. *Journal of Geophysical Research: Atmospheres*, *121*(12), 7117–7138. https://doi.org/10.1002/2016JD024783

Dunion, J. P. (2011). Rewriting the climatology of the tropical North Atlantic and Caribbean Sea atmosphere. *Journal of Climate*, *24*(3), 893–908. https://doi.org/10.1175/2010JCLI3496.1

Dunion, J. P., & Velden, C. S. (2004). The impact of the Saharan air layer on Atlantic tropical cyclone activity. *Bulletin of the American Meteorological Society*, *85*(3), 353–365. https://doi.org/10.1175/BAMS-85-3-353

Evan, A. T., Heidinger, A. K., Bennartz, R., Bennington, V., Mahowald, N. M., Corrada-Bravo, H., … Kossin, J. P. (2008). Ocean temperature forcing by aerosols across the Atlantic tropical cyclone development region. *Geochemistry, Geophysics, Geosystems*, *9*, Q05V04. https://doi.org/10.1029/2007GC001774

Gálvez, J. M., & Davison, M. (2014a). Gálvez-Davison Index calculation, accessed 2 April 2017. Retrieved from: http://www.wpc.ncep.noaa.gov/international/gdi/GDI_Calculation_Algorithm_20140702.pdf

Gálvez, J. M., & Davison, M. (2014b). The Gálvez-Davison index for tropical convection. 26th Conf. on Weather Analysis and Forecasting, Atlanta, GA, 2–6 February.

Gálvez, J. M., & Davison, M. (2016). The Gálvez-Davison Index for tropical convection, accessed 10 July 2017. Retrieved from: http://www.wpc.ncep.noaa.gov/international/gdi/GDI_Manuscript_V20161021.pdf

Gamble, D. (2014). The neglected climatic hazards of the Caribbean: Overview and prospects in a warmer climate. *Geography Compass*, *8*(4), 221–234. https://doi.org/10.1111/gec3.12125

Gamble, D. W., Parnell, D. B., & Curtis, S. (2008). Spatial variability of the Caribbean mid-summer drought and relation to North Atlantic high circulation. *International Journal of Climatology*, *28*(3), 343–350. https://doi.org/10.1002/joc.1600

Giannini, A., Chiang, J. C., Cane, M. A., Kushnir, Y., & Seager, R. (2001). The ENSO teleconnection to the tropical Atlantic Ocean: Contributions of the remote and local SSTs to rainfall variability in the tropical Americas. *Journal of Climate*, *14*(24), 4530–4544. https://doi.org/10.1175/1520-0442(2001)014%3C4530:TETTTT%3E2.0.CO;2

Giannini, A., Kushnir, Y., & Cane, M. A. (2000). Interannual variability of Caribbean rainfall, ENSO, and the Atlantic Ocean. *Journal of Climate*, *13*(2), 297–311. https://doi.org/10.1175/1520-0442(2000)013%3C0297:IVOCRE%3E2.0.CO;2

Ginoux, P., Prospero, J., Torres, O., & Chin, M. (2004). Long-term simulation of global dust distribution with the GOCART model: Correlation with North Atlantic Oscillation. *Environmental Modelling and Software*, *19*(2), 113–128. https://doi.org/10.1016/S1364-8152(03)00114-2

Glenn, E., Comarazamy, D., González, J. E., & Smith, T. (2015). Detection of recent regional sea surface temperature warming in the Caribbean and surrounding region. *Geophysical Research Letters*, *42*, 6785–6792. https://doi.org/10.1002/%202015GL065002

Goudie, A., & Middleton, N. (2001). Saharan dust storms: Nature and consequences. *Earth Science Reviews*, *56*(1-4), 179–204. https://doi.org/10.1016/S0012-8252(01)00067-8

Gouirand, I., Jury, M. R., & Sing, B. (2012). An analysis of low- and high-frequency summer climate variability around the Caribbean Antilles. *Journal of Climate*, *25*(11), 3942–3952. https://doi.org/10.1175/JCLI-D-11-00269.1

Guo, L., Highwood, E. J., Shaffrey, L. C., & Turner, A. G. (2013). The effect of regional changes in anthropogenic aerosols on rainfall of the East Asian Summer Monsoon. *Atmospheric Chemistry and Physics*, *13*(3), 1521–1534. https://doi.org/10.5194/acp-13-1521-2013

Hastenrath, S. (1967). Rainfall distribution and regime in Central America. *Archiv für Meteorologie, Geophysik und Bioklimatologie*, *15B*, 201–241.

Heartsill-Scalley, T., Scatena, F., Estrada, C., McDowell, W., & Lugo, A. (2007). Disturbance and long-term patterns of rainfall and throughfall nutrient fluxes in a subtropical wet forest in Puerto Rico. *Journal of Hydrology*, *333*(2-4), 472–485. https://doi.org/10.1016/j.jhydrol.2006.09.019

Hernández Ayala, J. J., & Matyas, C. J. (2016). Tropical cyclone rainfall over Puerto Rico and its relations to environmental and storm-specific factors. *International Journal of Climatology*, *36*(5), 2223–2237. https://doi.org/10.1002/joc.4490

Huang, J., Zhang, C., & Prospero, J. M. (2010). African dust outbreaks: A satellite perspective of temporal and spatial variability over the tropical Atlantic Ocean. *Journal of Geophysical Research*, *115*, D05202. https://doi.org/10.1029/2009JD012516

Huneeus, N., Schulz, M., Balkanski, Y., Griesfeller, J., Kinne, S., Porspero, J., … Zender, C. (2011). Global dust model intercomparison in AeroCom phase I. *Atmospheric Chemistry and Physics*, *11*(15), 7781–7816. https://doi.org/10.5194/acp-11-7781-2011

Inness, A., Baier, F., Benedetti, A., Bouarar, I., Chabrillat, S., Clark, H., … The MACC Team (2013). The MACC reanalysis: An 8-yr data set of atmospheric composition. *Atmospheric Chemistry and Physics*, *13*(8), 4073–4109. https://doi.org/10.5194/acp-13-4073-2013

Jury, M., Malmgren, B. A., & Winter, A. (2007). Subregional precipitation climate of the Caribbean and relationships with ENSO and NAO. *Journal of Geophysical Research*, *112*, D16107. https://doi.org/10.1029/2006JD007541

Jury, M. R. (2012). Representation of the Caribbean mean diurnal cycle in observation, reanalysis, and CMIP3 model datasets. *Theoretical and Applied Climatology*, *107*(1–2), 313–324. https://doi.org/10.1007/s00704-011-0462-4

Jury, M. R., & Gouirand, I. (2011). Decadal climate variability in the eastern Caribbean. *Journal of Geophysical Research*, *116*, D00Q03. https://doi.org/10.1029/2010JD015107

Jury, M. R., & Santiago, M. J. (2010). Composite analysis of dust impacts on African easterly waves in the Moderate Resolution Imaging Spectrometer era. *Journal of Geophysical Research*, *115*, D16213. https://doi.org/10.1029/2009JD013612

Karmalkar, A. V., Taylor, M. A., Campbell, J., Stephenson, T., New, M., Centella, A., … Charlery, J. (2013). A review of observed and projected changes in climate for the islands in the Caribbean. *Atmosfera*, *26*(2), 283–309. https://doi.org/10.1016/S0187-6236(13)71076-2

Khain, A. P. (2009). Notes on state-of-the-art investigations of aerosol effects on precipitation: A critical review. *Environmental Research Letters*, *4*(1), 015004. https://doi.org/10.1088/1748-9326/4/1/015004

Larsen, M. C. (2000). Analysis of 20th century rainfall and streamflow to characterize drought and water resources in Puerto Rico. *Physical Geography*, *21*, 494–521.

Livezey, R. E., & Chen, W. Y. (1983). Statistical field significance and its determination by Monte Carlo techniques. *Monthly Weather Review*, *111*(1), 46–59. https://doi.org/10.1175/1520-0493(1983)111%3C0046:SFSAID%3E2.0.CO;2

Magañ, V., Amador, J. A., & Medina, S. (1999). The midsummer drought over Mexico and Central America. *Journal of Climate*, *12*(6), 1577–1588. https://doi.org/10.1175/1520-0442(1999)012%3C1577:TMDOMA%3E2.0.CO;2

Malmgren, B. A., Winter, A., & Chen, D. (1998). El Niño–Southern Oscillation and North Atlantic Oscillation control of climate in Puerto Rico. *Journal of Climate*, *11*(10), 2713–2717. https://doi.org/10.1175/1520-0442(1998)011%3C2713:ENOSOA%3E2.0.CO;2

Meng, L., Gao, H. W., Yu, Y., Yao, X. H., Gao, Y., Zhang, C., & Fan, L. (2017). A new approach developed to study variability in North African dust transport routes over the Atlantic during 2001–2015. *Geophysical Research Letters*, *44*. https://doi.org/10.1002/2017GL074478

National Drought Mitigation Center (2016). U.S. Drought Monitor map archive, accessed 21 August 2016. Retrieved from: http://drought-monitor.unl.edu/MapsAndData/MapArchive.aspx

NOAA National Centers for Environmental Information (2015). State of the climate: Drought for July 2015. accessed 2 April 2017. Retrieved from: http://www.ncdc.noaa.gov/sotc/drought/201507

NOAA Weather Prediction Center (2016). Experimental Gálvez-Davison Index (GDI), accessed 2 April 2017. Retrieved from: http://www.wpc.ncep.noaa.gov/international/gdi/

Pasch, R. J., & Penny, A. B. (2016). Danny (AL052015) National Hurricane Center Tropical Cyclone Report, 18, NOAA National Hurricane Center.

Patricola, C. M., Chang, P., & Saravanan, R. (2016). Degree of simulated suppression of Atlantic tropical cyclones modulated by flavour of El Nino. *Nature Geoscience*, *9*(2), 155–160. https://doi.org/10.1038/ngeo2624

Petit, R. H., Legrand, M., Jankowiak, I., Molinié, J., Asselin de Beauville, C., Marion, G., & Mansot, J. L. (2005). Transport of Saharan dust over the Caribbean Islands: Study of an event. *Journal of Geophysical Research*, *110*, D18S09. https://doi.org/10.1029/2004JD004748

Prospero, J. M., Ginoux, P., Torres, O., Nicholson, S. E., & Gill, T. E. (2002). Environmental characterization of global sources of atmospheric soil dust identified with the NIMBUS 7 Total Ozone Mapping Spectrometer (TOMS) absorbing aerosol product. *Reviews of Geophysics*, *40*(1), 1002. https://doi.org/10.1029/2000RG000095

Prospero, J. M., & Mayol-Bracero, O. L. (2013). Understanding the transport and impact of African dust on the Caribbean Basin. *Bulletin of the American Meteorological Society*, *94*(9), 1329–1337. https://doi.org/10.1175/BAMS-D-12-00142.1

Ramage, C. S. (1995). Forecasters guide to tropical meteorology. Updated. Tech. Rept. AWS/TR-95/001, Air Weather Service Scott AFB IL, 492.

Rao, C. R. N., Stowe, L. L., & McClain, E. P. (1989). Remote sensing of aerosols over the oceans using AVHRR data—Theory, practice and applications. *International Journal of Remote Sensing*, *10*, 743–749.

Reid, J. S., Kinney, J. E., Westphal, D. L., Holben, B. N., Welton, E. J., Tsay, S.-C., … Tanré, D. (2003). Analysis of measurements of Saharan dust by airborne and ground-based remote sensing methods during the Puerto Rico Dust Experiment (PRIDE). *Journal of Geophysical Research*, *108*(D19), 8586. https://doi.org/10.1029/2002JD002493

Ropelewski, C. F., & Halpert, M. S. (1987). Global and regional scale precipitation patterns associated with the El Niño/Southern Oscillation. *Monthly Weather Review*, *115*(8), 1606–1626. https://doi.org/10.1175/1520-0493(1987)115%3C1606:GARSPP%3E2.0.CO;2

Ropelewski, C. F., & Halpert, M. S. (1996). Quantifying southern oscillation-precipitation relationships. *Journal of Climate*, *9*(5), 1043–1059. https://doi.org/10.1175/1520-0442(1996)009%3C1043:QSOPR%3E2.0.CO;2

Rosenfeld, D., Rudich, Y., & Lahav, R. (2001). Desert dust suppressing precipitation: A possible desertification feedback loop. *Proceedings of the National Academy of Sciences*, *98*(11), 5975–5980. https://doi.org/10.1073/pnas.101122798

Scatena, F. N. (1995). Relative scales of time and effectiveness of watershed processes in a tropical montane rain forest of Puerto Rico. *Geophysical Monograph Series Natural and Anthropogenic Influences in Fluvial Geomorphology*, *89*. https://doi.org/10.1029/GM089p0103

Schepanski, K., Tegen, I., & Macke, A. (2012). Comparison of satellite based observations of Saharan dust source areas. *Remote Sensing of Environment*, *123*, 90–97. https://doi.org/10.1016/j.rse.2012.03.019

Stewart, S. R. (2016). Hurricane Danny (AL042015) National Hurricane Center Tropical Cyclone Report, 18, NOAA National Hurricane Center.

Taylor, M. A., Enfield, D. B., & Chen, A. A. (2002). Influence of the tropical Atlantic versus the tropical Pacific on Caribbean rainfall. *Journal of Geophysical Research*, *107*(C9), 3127. https://doi.org/10.1029/2001JC001097

Taylor, M. A., Stephenson, T. S., Owino, A., Chen, A. A., & Campbell, J. D. (2011). Tropical gradient influences on Caribbean rainfall. *Journal of Geophysical Research*, *116*, D00Q08. https://doi.org/10.1029/2010JD015580

Thornton, P. E., Running, S. W., & White, M. A. (1997). Generating surfaces of daily meteorological variables over large regions of complex terrain. *Journal of Hydrology*, *190*(3–4), 214–251. https://doi.org/10.1016/S0022-1694(96)03128-9

Thornton, P. E., Thornton, M. M., Mayer, B. W., Wei, Y., Devarakonda, R., Vose, R. S., & Cook, R. B. (2017). Daymet: Daily surface weather data on a 1-km grid for North America, version 3 ORNL DAAC, Oak Ridge, TN.

Torres, O., Tanskanen, A., Veihelmann, B., Ahn, C., Braak, R., Bhartia, P. K., … Levelt, P. (2007). Aerosols and surface UV products from Ozone Monitoring Instrument observations: An overview. *Journal of Geophysical Research*, *112*, D24S47. https://doi.org/10.1029/2007JD008809

U.S. Department of Agriculture (USDA) (2015). Historic drought in Puerto Rico affecting 2.7 million people. accessed 21 August 2016. Retrieved from http://www.climatehubs.oce.usda.gov/content/historic-drought-puerto-rico-affecting-2-7-million-people

U.S. Geological Survey (USGS) (2016). Hydrologic conditions of selected reservoirs in Puerto Rico, accessed 21 August 2016. Retrieved from http://pr.water.usgs.gov/drought/hydro_conditions_selected_sites.html

USGS (2016). Water watch, accessed 21 August 2016. Retrieved from: http://waterwatch.usgs.gov/

Van Beusekom, A. E., González, G., & Rivera, M. M. (2015). Short-term precipitation and temperature trends along an elevation gradient in northeastern Puerto Rico. *Earth Interactions*, *19*(3), 1–33. https://doi.org/10.1175/EI-D-14-0023.1

Wong, S., & Dessler, A. E. (2005). Suppression of deep convection over the tropical North Atlantic by the Saharan Air Layer. *Geophysical Research Letters*, *32*, L09808. https://doi.org/10.1029/2004GL022295

Wong, S., Dessler, A. E., Mahowald, N. M., Colarco, P. R., & Silva, A. D. (2008). Long-term variability in Saharan dust transport and its link to North Atlantic sea surface temperature. *Geophysical Research Letters*, *35*, L07812. https://doi.org/10.1029/2007GL032297

Wu, R., & Kirtman, B. P. (2011). Caribbean Sea rainfall variability during the rainy season and relationship to the equatorial Pacific and tropical Atlantic SST. *Climate Dynamics*, *37*(7–8), 1533–1550. https://doi.org/10.1007/s00382-010-0927-7

Xie, P., & Arkin, P. A. (1997). Global precipitation: A 17-year monthly analysis based on gauge observations, satellite estimates, and numerical model outputs. *Bulletin of the American Meteorological Society*, *78*(11), 2539–2558. https://doi.org/10.1175/1520-0477(1997)078%3C2539:GPAYMA%3E2.0.CO;2